A highly redox-heterogeneous ocean in South China during the early Cambrian (∼529–514 Ma): Implications for biota-environment co-evolution

Chengsheng Jin [a], Chao Li [a,*], Thomas J. Algeo [a,b,c], Noah J. Planavsky [d], Hao Cui [a], Xinglian Yang [e], Yuanlong Zhao [e], Xingliang Zhang [f], Shucheng Xie [a]

[a] *State Key Laboratory of Biogeology and Environmental Geology, China University of Geosciences, Wuhan 430074, China*
[b] *State Key Laboratory of Geological Processes and Mineral Resources, China University of Geosciences, Wuhan 430074, China*
[c] *Department of Geology, University of Cincinnati, Cincinnati, OH 45221-0013, USA*
[d] *Department of Geology and Geophysics, Yale University, New Haven, CT 06520, USA*
[e] *College of Resource and Environment, Guizhou University, Guiyang 550003, China*
[f] *Early Life Institute and State Key Laboratory for Continental Dynamics, Department of Geology, Northwest University, Xi'an 710069, China*

A B S T R A C T

The "Cambrian Explosion" is known for rapid increases in the morphological disparity and taxonomic diversity of metazoans. It has been widely proposed that this biological event was a consequence of oxygenation of the global ocean, but this hypothesis is still under debate. Here, we present high-resolution Fe–S–C–Al-trace element geochemical records from the Jinsha (outer shelf) and Weng'an (outer shelf) sections of the early Cambrian Yangtze Platform, integrating these results with previously published data from six correlative sections representing a range of water depths (Xiaotan, Shatan, Dingtai, Yangjiaping, Songtao, and Longbizui). The integrated iron chemistry and redox-sensitive trace element data suggest that euxinic mid-depth waters dynamically coexisted with oxic surface waters and ferruginous deep waters during the earliest Cambrian, but that stepwise expansion of oxic waters commenced during Cambrian Stage 3 (∼521–514 Ma). Combined with data from lower Cambrian sections elsewhere, including Oman, Iran and Canada, we infer that the global ocean exhibited a high degree of redox heterogeneity during the early Cambrian, consistent with low atmospheric oxygen levels (∼10–40% of present atmospheric level, or PAL). A large spatial gradient in pyrite sulfur isotopic compositions ($\delta^{34}S_{py}$), which vary from a mean of −12.0‰ in nearshore areas to +22.5‰ in distal deepwater sections in lower Cambrian marine units of South China imply low concentrations and spatial heterogeneity of seawater sulfate, which is consistent with a limited oceanic sulfate reservoir globally. By comparing our reconstructed redox chemistry with fossil records from the lower Cambrian of South China, we infer that a stepwise oxygenation of shelf and slope environments occurred concurrently with a gradual increase in ecosystem complexity. However, deep waters remained anoxic and ferruginous even as macrozooplankton and suspension-feeding mesozooplankton appeared during Cambrian Stage 3. These findings suggest that the "Cambrian Explosion" in South China may have been primarily a consequence of locally improved oxygenation of the ocean-surface layer rather than of the full global ocean. Our observations are inconsistent with predicted changes in ocean chemistry driven by early Cambrian animals, suggesting that the influence of early Cambrian animals on contemporaneous ocean chemistry, as proposed in previous studies, may be overly exaggerated.

1. Introduction

The early Cambrian was a key period in the evolution of life and environmental changes on Earth. Following the extinction of the Ediacaran biota near the Precambrian–Cambrian boundary, a rapid diversification of animals occurred during the early Cambrian. The appearance of small shelly fossil assemblages (SSFAs) during Cambrian Fortunian Stage and Stage 2 signaled the advent of widespread biomineralization and a radiation among bilaterians (e.g., Steiner et al., 2007; Zhu, 2010; Landing et al., 2013; Shu et al., 2014). These faunas were subsequently replaced dur-

ing Cambrian Stage 3 by the Chengjiang Biota, which was characterized by increased phyletic diversity and ecospace utilization (e.g., Knoll and Carroll, 1999; Zhu, 2010; Shu et al., 2014). There are three competing views regarding cause-and-effect relationships between oceanic oxygenation and biological radiation during the early Cambrian. The conventional view argues that an oxygen rise in the early Cambrian atmosphere–ocean system stimulated a rapid diversification of animals (Knoll and Carroll, 1999). A recent Mo-isotope study provides evidence for near-modern oxygen levels at ∼521 Ma, which might have driven the subsequent metazoan radiation (X. Chen et al., 2015). The second view is that ventilation of the deep ocean (i.e., below the surface mixed layer) during the early Cambrian was a consequence of the evolution of macrozooplankton and suspension-feeding mesozooplankton, which increased the sinking and burial fluxes of organic matter and triggered a comprehensive biogeochemical reorganization of the oceans (e.g., Logan et al., 1995; Butterfield, 2009). Recently, Boyle et al. (2014) instead argued that a rise in bioturbation intensity during Cambrian Stage 2 enhanced organic phosphate burial, leading to a reduced seawater phosphate reservoir, lower primary production, and reduced organic carbon burial, thus triggering a decline in atmosphere–ocean oxygen concentrations and expansion of ocean anoxia during Cambrian Stages 3 and 4. The third view is that there was no specific relationship between atmosphere–ocean oxygen levels and the "Cambrian Explosion" (e.g., Mills and Canfield, 2014).

Oxygenation of the global deep ocean is inferred to have begun during the onset of the Neoproterozoic Bitter Springs stage (∼811.5 Ma) (Thomson et al., 2015) and to have continued through the rest of the Neoproterozoic with rises and falls (e.g., Kendall et al., 2015; Turner and Bekker, 2016; Wang et al., 2015). Significant increases in marine sediment Mo and U concentrations as well as in δ^{98}Mo values (to $+2.34‰$, or as high as modern seawater $\delta^{98/95}$Mo) implied strong oxygenation of the deep oceans at the base of Cambrian Stage 3 (X. Chen et al., 2015), when atmospheric oxygen levels may have risen to near-modern values (Berner, 2009). However, anoxic waters are thought to have still existed widely in early Cambrian oceans based on geochemical proxies such as iron chemistry (Goldberg et al., 2007; Canfield et al., 2008; Sperling et al., 2015), redox-sensitive elements (Kimura and Watanabe, 2001; Guo et al., 2007; Schröder and Grotzinger, 2007; Rajabi et al., 2015), and framboidal pyrite (Rajabi et al., 2015), concurrently with atmospheric oxygen levels of ∼10–40% PAL (Sperling et al., 2015). Recent study of spatial patterns of Fe–Mo–S–C variation in lower Cambrian marine units of the Yangtze Block in South China support a highly stratified early Cambrian ocean, in which mid-depth euxinic waters were dynamically maintained in proximity to oxic surface waters and ferruginous deep waters (Feng et al., 2014). This finding on the spatial heterogeneity of ocean chemistry complicate, but potentially shed new light on, the ongoing debate about the relationship between oceanic oxygenation and metazoan radiation during the early Cambrian.

In this study, we explore in detail the relationship between spatiotemporal variation in redox conditions of the early Cambrian Yangtze Block and concurrent bio-evolutionary changes to test the three competing views given above. We conducted a high-resolution chemostratigraphic study of two outer-shelf sections (Jinsha and Weng'an) on the Yangtze Platform, generating new Fe speciation, redox-sensitive trace element (RSTE) concentration (Mo, U, V), and pyrite sulfur isotope data that were combined with published data from six other sections representing a range of paleo-water depths from inner-shelf to slope. This integrated dataset provided us a unique spatiotemporal framework within which to evaluate the co-evolution of oceanic redox conditions and early metazoan during the early Cambrian.

2. Geological setting

2.1. Paleogeography and section locations

South China was an isolated craton at mid-Northern Hemisphere latitudes during the early Cambrian (Fig. 1A; Li et al., 2008). It consisted of the Yangtze and Cathaysia tectonic blocks, which were sutured together during the mid-Neoproterozoic and which underwent failed rifting during the late Neoproterozoic, producing the Nanhua Basin between them (Fig. 1B; Wang and Li, 2003). The Nanhua Basin is thought to have been in effective communication with the open ocean during the early Cambrian based on (1) global paleogeographic reconstructions of South China as an isolated craton surrounded by the open ocean (Fig. 1A; Li et al., 2008), (2) the occurrence of the same or similar fossils (e.g., small shelly fossils and arthropods) in South China and elsewhere globally, including Siberia, West Avalonia, and Greenland (e.g., Steiner et al., 2007; Vannier et al., 2014), and (3) similar carbonate carbon isotope profiles for the Cambrian Fortunian Stage and lower Stage 2 in South China and age-equivalent sections globally (e.g., Siberia, Morocco, and Mongolia) (e.g., Ishikawa et al., 2008).

Upper Ediacaran to lower Cambrian (∼551–529 Ma) strata of the Yangtze Block exhibit three broad sedimentary facies belts, from northwest to southeast: (1) shallow-water deposits of the Yangtze Platform, (2) slope, and (3) deep-water deposits of the Nanhua Basin (Fig. 1B; Zhu et al., 2003; Steiner et al., 2007). During the late Ediacaran to early Cambrian (Fortunian-lower Stage 2), shallow-water areas accumulated mainly dolomite (Dengying Formation and lower-middle Zhujiaqing Formation) and interbedded limestone and phosphorite (lower-middle Zhujiaqing Formation and stratigraphic equivalents). The correlative strata in the transitional zone are mainly dolomite (Dengying Formation) and interbedded limestone and shale/mudstone (lower Niutitang Formation and stratigraphic equivalents). Deep-water areas accumulated mainly chert (Liuchapo Formation and equivalents) and shale (lower Niutitang Formation and equivalents). As a consequence of a major marine transgression, black shales were deposited over the entire Yangtze Block in the upper Meishucunian-lower Qiongzhusian (i.e., upper Stage 2-lower Stage 3; Zhu et al., 2003).

The two main study sections are Jinsha (27°32′50″N and 106°16′39″E, northwestern Guizhou Province) and Weng'an (27°04′0.4″N and 107°34′45.3″E, central Guizhou Province), which have well-studied biostratigraphic records (see Section 2.2), offering a unique opportunity for evaluating biota-environment co-evolution in an outer-shelf setting—a key area for the chemical evolution of seawater during the early Cambrian (Feng et al., 2014). The six previously studied auxiliary sections are Xiaotan (inner shelf; northeastern Yunnan; Och et al., 2013), Shatan (inner shelf; Sichuan; Goldberg et al., 2007; Guo et al., 2007), Dingtai (outer shelf; Guizhou; Xu et al., 2012), Yangjiaping (outer shelf; Hunan; Feng et al., 2014), Songtao (slope; Guizhou; Goldberg et al., 2007; Guo et al., 2007; Canfield et al., 2008), and Longbizui (slope; Hunan; Wang et al., 2012a). These eight sections are distributed along two intersecting shelf-to-basin transects across the Yangtze Block: A–A′ from northwest to southeast and B–B′ from west to east (Fig. 1B).

2.2. Lithostratigraphy and biostratigraphy

The lower Cambrian successions of the outer-shelf Jinsha and Weng'an sections consist of the Niutitang and Mingxinsi formations, which unconformably overlie the late Ediacaran Dengying Formation (Fig. 2). The Niutitang Formation is subdivided into two members: (1) a lower member consisting of black shale, and (2) an upper member consisting of shales, mudstone, muddy siltstone, calcareous mudstone, and silty mudstone. The Mingxinsi
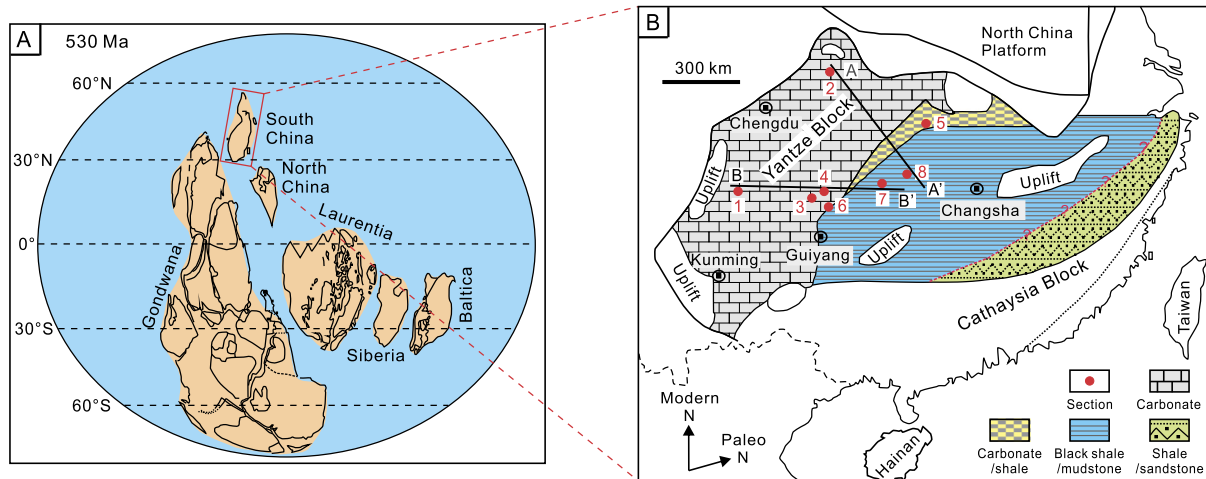
Fig. 1. (A) Early Cambrian global paleogeography (modified from Li et al., 2008). Note that the Yangtze Block was rotated about 80° counter-clockwise relative to its modern orientation. (B) Paleoenvironmental map of the Nanhua Basin during the early Cambrian (Fortunian and early Stage 2/early–middle Meishucunian stages) (modified from Goldberg et al., 2007). Sections: 1 – Xiaotan, 2 – Shatan, 3 – Jinsha, 4 – Dingtai, 5 – Yangjiaping, 6 – Weng'an, 7 – Songtao, and 8 – Longbizui. Note that the sections are approximately aligned along two shelf-to-basin transects (A–A′ and B–B′).

Formation, which conformably overlies the Niutitang Formation, is composed mainly of mudstone and muddy limestone at Jinsha and muddy limestone interbedded with calcareous mudstone at Weng'an.

At Jinsha, the lower member of the Niutitang Formation contains various fossils such as the trilobites *T. armatus* and *T. niutitangensis*, the bivalved arthropods *Kunmingella douvillei* and *Tsunyiella* cf. *luna*, and the sponge *Leptomitus teretiusulus* (Yang et al., 2014; Zheng et al., 2014). Because the fossil assemblage is dominated by sponges, it is known as the Niutitang Sponge Fauna (Zhu, 2010). In contrast, the upper member of the Niutitang Formation contains a trilobite-rich assemblage including *T. armatus, T. niutitangensis*, *Zhenbaspis*, and *Qingkouia zhangyangouensis* (Zhang et al., 1979; Zheng et al., 2014). The Mingxinsi Formation contains abundant trilobites such as *Kueichowia*, *Drepanuroides*, and *Mayiella* (Zhang et al., 1979).

At Weng'an, the lower member of the Niutitang Formation contains the trilobites *T. armatus* and *T. niutitangensis*, rhabdopleurides, and sponges, and the upper member contains the trilobite *Sinodiscus shipaiensis* (Yang et al., 2003). The Mingxinsi Formation yielded the trilobites *Hupeidiscus orientalis*, *Hunanocephalus* sp., and *Metaredlichia* sp. (Yang et al., 2003).

A detailed summary of the lithostratigraphy and biostratigraphy of the previously studied Xiaotan, Shatan, Dingtai, Yangjiaping, Songtao, and Longbizui sections can be found in Supplementary Online Material (SOM) S1.1. The geochronological frameworks for these sections can be found in the SOM S1.2.

2.3. Stratigraphic correlation of study sections

Based on litho- and biostratigraphic data, post-Fortunian lower Cambrian strata of the eight study sections can be correlated within a framework of four stratigraphic intervals (Fig. 2), which represent the major stages of basin sedimentology and biological evolution (see SOM Section S1.1 and Section 5). Interval I extends from the base of the black shales of the Niutitang Formation and its stratigraphic equivalents upward to the widely occurring Ni–Mo layer in shelf sections (i.e., Xiaotan, Shatan, Jinsha, and Weng'an) or the "stone coal" in slope sections (i.e., Songtao and Longbizui). The correlations of shelf sections are based on similar lithologic markers or/and the first appearance of the trilobite *T. niutitangensis* just above the Ni–Mo layer. Correlation of this interval into the basin is based on the well-established equivalency of the Ni–Mo

layer with the "stone coal" (e.g., Yang et al., 2003; Zhu et al., 2003; D. Chen et al., 2015). However, the top of Interval I cannot be precisely located in the outer-shelf Yangjiaping section due to absence of the Ni–Mo layer.

Interval II ranges from the top of Interval I upward to the top of the black shale succession in the shelf sections (i.e., Xiaotan, Shatan, Jinsha, and Dingtai). In these sections, the top of Interval II is based on (1) occurrences of the trilobite *Eoredlichia* at Shatan and in sections close to Xiaotan (i.e., Jinning and Haikou) (Luo et al., 1994; Yin et al., 1999), and (2) similar fossils (e.g., *Naraoia* and *Isoxys*) of the Chengjiang Biota in sections close to Xiaotan (i.e., Haikou) and of the Zunyi Biota in the Zhongnan section close to Dingtai, which appear immediately above the black shale succession (Luo et al., 1997; Zhao et al., 1999). Because the first appearance of the trilobite *Q. zhangyangouensis* is younger than that of the trilobite *Eoredlichia* (Yuan and Zhao, 1999), the top of Interval II must be below beds containing *Q. zhangyangouensis* at Jinsha (Zhang et al., 1979). However, stratigraphic markers for the top of Interval II are absent in the deep-water Yangjiaping, Weng'an, Songtao, and Longbizui sections.

Interval III ranges from the top of Interval II upward to the top of the Qiongzhusian. The top of Interval III is correlated among the study sections based mainly on (1) similar trilobites *Mayiella* and *Drepanuroides* at Jinsha and in a section near Xiaotan (i.e., Malong), (2) the trilobites *Kuweichowia* sp., *Mayiella*, and *Drepanuroides* sp. at Jinsha, as well as the trilobites *Hupeidiscus* sp. and *Metaredlichia* sp. at both Weng'an and Songtao, since these trilobites are markers of the Qiongzhusian–Canglangpuian boundary (Yuan and Zhao, 1999; Yang et al., 2003). Because the first appearance of the trilobite *Hunanocephalus* sp. indicates a late Qiongzhusian or early Canglangpuian age (Yuan and Zhao, 1999), the top of Interval III must be within or close to beds containing *Hunanocephalus* sp. at Yangjiaping (Yin et al., 1999). The top of Interval III at Longbizui may be located near the top of the black shale succession because of similarities in thickness, lithology, and biotic changes with the nearby Songtao section. Interval IV is defined as the strata overlying Interval III, and the top of this interval was not determined in the present study.

We note that some uncertainties remain regarding the correlations discussed above due to the absence of global stratotype sections and points (GSSPs) for Cambrian Stages 2 and 3, the possible existence of local stratigraphic hiatuses in some study sections, and the general complexity of the litho- and biostratig-
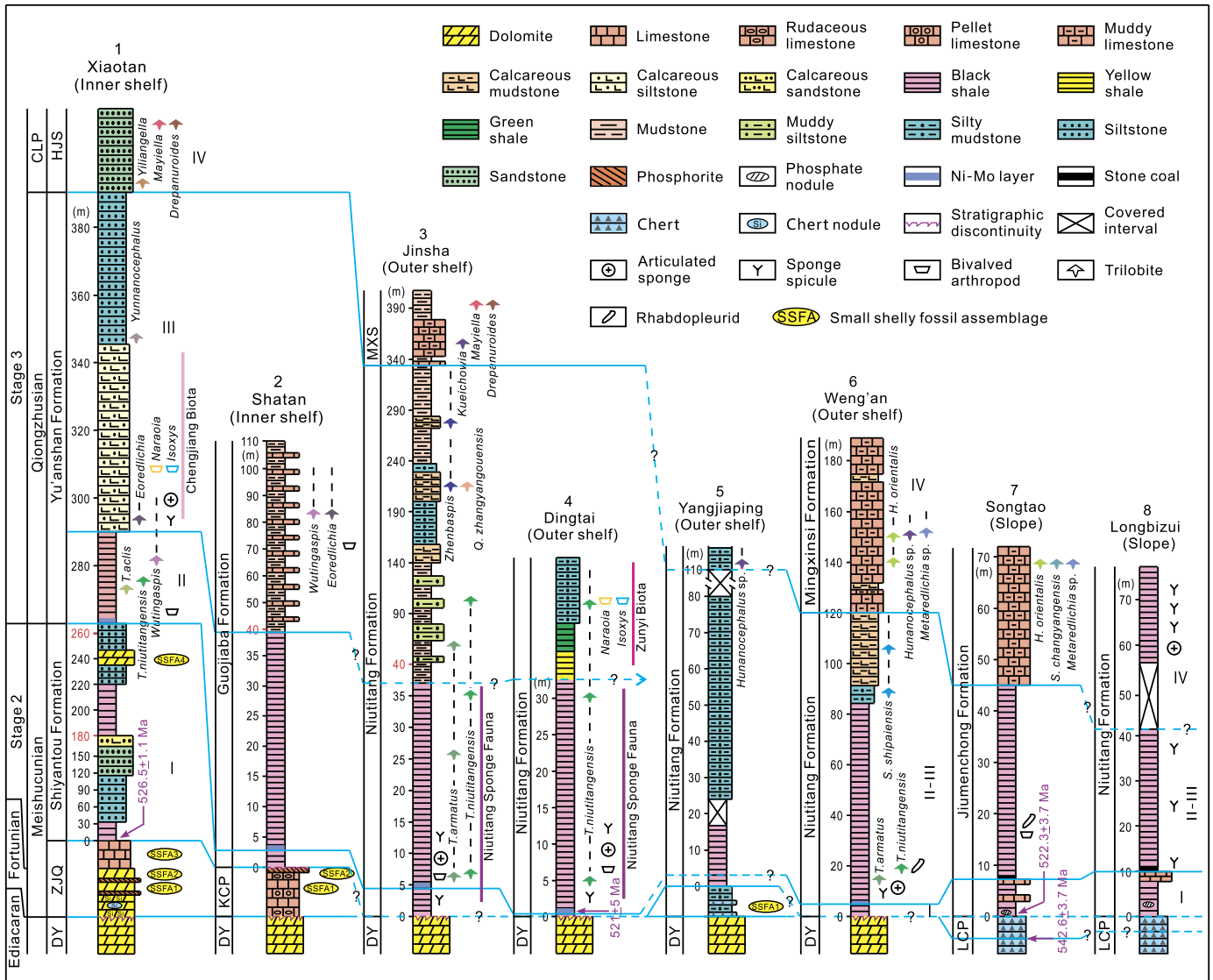
Fig. 2. Stratigraphic framework for early Cambrian strata (∼541–514 Ma) of the Yangtze Block. I to IV denote stratigraphic intervals discussed in the text. Note changes in the vertical scales of the Xiaotan, Shatan, and Jinsha sections (denoted by red numbers). Sources of litho- and biostratigraphic data: 1 – Xiaotan (Chen et al., 1990; Luo et al., 1994, 1997; Yang et al., 2003; Li and Xiao, 2004; Och et al., 2013); 2 – Shatan (Yin et al., 1999; Goldberg et al., 2007); 3 – Jinsha (Zhang et al., 1979; Yang et al., 2014; Zheng et al., 2014; this study); 4 – Dingtai (Zhao et al., 1999; Xu et al., 2012); 5 – Yangjiaping (Yin et al., 1999; Feng et al., 2014); 6 – Weng'an (Yang et al., 2003; this study); 7 – Songtao (Yang et al., 2003; Goldberg et al., 2007); 8 – Longbizui (Wang et al., 2012a; Guo et al., 2013). U–Pb age data for the Xiaotan and Songtao sections are from the adjacent Meishucun (Compston et al., 2008) and Bahuang sections (D. Chen et al., 2015), respectively. The Re–Os age of the Ni–Mo layer at Dingtai is based on data from Sancha, Maluhe, and Dazhuliushui (Xu et al., 2011). Abbreviations: CLP = Canglangpuian Stage, DY = Dengying Formation, HJS = Hongjingshao Formation, KCP = Kuanchuanpu Formation, LCP = Liuchapo Formation, MXS = Mingxinsi Formation, and ZJQ = Zhujiaqing Formation. (For interpretation of the references to color in this figure legend, the reader is referred to the web version of this article.)

raphy of the early Cambrian Yangtze Block (e.g., Yang et al., 2003; Zhu et al., 2003). However, our chronostratigraphic framework is sufficiently robust as to provide a useful basis for spatiotemporal analysis of early Cambrian ocean chemistry in South China and its relationship to the "Cambrian Explosion" (Yang et al., 2003; Zhu et al., 2003).

3. Background: iron speciation, redox-sensitive trace elements as paleoredox proxies

Sedimentary iron speciation is widely used as an indicator of paleoceanic redox conditions (e.g., Canfield et al., 2008; Li et al., 2010, 2012; Poulton and Canfield, 2011). Modern and ancient marine sediments deposited under an anoxic water column are generally characterized by highly reactive iron (Fe$_{HR}$) vs. total iron

(Fe$_T$) > 0.38 (Raiswell and Canfield, 1998). Here, the Fe$_{HR}$ is a sum of pyrite Fe (Fe$_{py}$), carbonate-associated Fe (Fe$_{carb}$), ferric oxide Fe (Fe$_{ox}$) and magnetite Fe (Fe$_{mag}$). When anoxia is inferred, Fe$_{py}$/Fe$_{HR}$ exceeding 0.7–0.8 is consistent with a euxinic water column (Poulton and Canfield, 2011). These threshold values are regarded as more reliable for siliciclastic rocks than for other lithologies (Lyons and Severmann, 2006), although they are also applicable to carbonate rocks with Fe$_T$ > 0.5% (Clarkson et al., 2014).

We also used RSTE concentrations (Mo, U, V) as an independent paleoredox proxy. In general, RSTEs become less soluble or more particle-reactive under reducing conditions, resulting in authigenic enrichment of the sediment relative to average upper continental crust (Tribovillard et al., 2006). Specifically, modern marine studies have shown that Mo concentrations are commonly <25 ppm for non-euxinic waters, 25–100 ppm for intermit-

tently/seasonally euxinic or Mo-limited permanently euxinic waters, and >100 ppm for permanently euxinic waters (see Scott and Lyons, 2012). Restricted-marine settings have limited RSTE resupply, which can reduce the degree of RSTE enrichment of the sediment even under strongly euxinic conditions (e.g., Scott and Lyons, 2012). However, in view of evidence for lack of watermass restriction within the early Cambrian Nanhua Basin (see Section 2.1), we infer that observed RSTE enrichments in the study sections are a robust proxy for local redox conditions (see Section 5).

4. Materials and methods

A total of 87 samples from the Jinsha and Weng'an sections were crushed to powder for Fe–S–C–Al-trace element geochemical analyses, which were conducted at the State Key Laboratory of Biogeology and Environmental Geology, China University of Geosciences (Wuhan). Details for the routine analytical methods, as well as errors and precisions for each analysis, are available in the SOM S2 for this paper, although a brief description of these methods is provided here.

Fe_{Py} was stoichiometrically calculated from the weight percentage of pyrite sulfur extracted as an Ag_2S precipitate using the Cr-reduction method (Canfield et al., 1986). Fe_{carb}, Fe_{ox}, and Fe_{mag} were recovered through a sequential extraction procedure as described by Poulton and Canfield (2005). The resulting Ag_2S precipitates from Cr-reduction were combined with an excess of V_2O_5 and combusted online for measuring the sulfur isotopic composition of pyrite ($\delta^{34}S_{Py}$) on a Thermo Fisher Scientific Delta V Plus isotope ratio mass spectrometer coupled with a Flash elemental analyzer. Trace elements and, for most samples, Fe_T and Al were determined using a standard $HF–HCl–HNO_3$ digestion which was followed by measurements using inductively-coupled-plasma-atomic-emission spectroscopy (ICP-AES) for Fe and Al concentrations, and quadrupole inductively coupled plasma mass spectroscopy (ICP-MS) for trace elements concentrations. For some samples, Fe_T concentrations were determined using an Olympus DP-6000 hand-held X-ray fluorescence spectroscope (HH-XRF) with a Rh tube, as described by Lenniger et al. (2014). Total organic carbon (TOC) was calculated by difference between total carbon (TC) and total inorganic carbon (TIC), which were measured by using a Jena multi-EA 4000 carbon–sulfur analyzer through online combustion at 1350 °C and acidification with ∼30–40% phosphoric acid, respectively.

5. Results and discussion

The Fe–S–C–Al-trace element geochemical data from the outer-shelf Jinsha and Weng'an sections of this study, as well as previously reported data from the inner-shelf Xiaotan (Och et al., 2013, in press), inner-shelf Shatan (Goldberg et al., 2007; Guo et al., 2007), outer-shelf Dingtai (Xu et al., 2012), outer-shelf Yangjiaping (Feng et al., 2014), slope Songtao (Goldberg et al., 2007; Guo et al., 2007; Canfield et al., 2008), and slope Longbizui sections (Wang et al., 2012a), are summarized in Table S1 and Figs. 3, 4 and 5. Below, we interpret redox patterns for the Jinsha and Weng'an sections (this study) and reassess redox proxy data for the Xiaotan and Dingtai sections, which were not fully evaluated in the original sources. Redox interpretations for the Shatan, Yangjiaping, Songtao, and Longbizui sections were fully discussed by Feng et al. (2014) and will not be duplicated here.

5.1. Reconstruction of paleomarine redox conditions

5.1.1. Redox conditions at Xiaotan (inner shelf)

Iron speciation and RSTE data for the Xiaotan section (Figs. 5A and 6) were originally reported by Och et al. (2013). For Interval I, these proxies ($Fe_T > 0.5\%$, Fe_{HR}/Fe_T: 0.36–0.93 and Fe_{Py}/Fe_{HR}:

0–0.18; U: mean 5 ppm, V: mean 411 ppm, and Mo: mean 8 ppm) suggest anoxic and ferruginous conditions from 0 to 36 m and from 180 to 222 m. Three samples from 232 to 252 m are characterized by low U (up to 2 ppm, mean 1 ppm), V (up to 62 ppm, mean 61 ppm), and Mo concentrations (up to 1 ppm, mean 1 ppm), possibly reflecting an episode of oxic conditions (Table S1).

For Interval II, Fe speciation data permit recognition of two units. Samples from 263.0 to 268.3 m are characterized by $Fe_T >$ 0.5%, high Fe_{HR}/Fe_T (0.40–0.51, mean 0.46), and low Fe_{Py}/Fe_{HR} (0–0.08, mean 0.03). These values imply ferruginous conditions, consistent with moderate U (up to 26 ppm, mean 11 ppm), V (up to 661 ppm, mean 514 ppm), and Mo concentrations (up to 39 ppm, mean 25 ppm). Samples from 268.3 to 288.5 m are characterized by $Fe_T > 0.5\%$, low Fe_{HR}/Fe_T (0.23–0.41, mean 0.33), and low Fe_{Py}/Fe_{HR} (0.02–0.18, mean 0.11). These values indicate dominantly oxic conditions, in agreement with low U (up to 6 ppm, mean 4 ppm) and Mo concentrations (up to 12 ppm, mean 5 ppm) and slightly elevated V concentrations (up to 483 ppm, mean 303 ppm).

For Interval III, almost all samples exhibit $Fe_T > 0.5\%$, low Fe_{HR}/Fe_T (0.22–0.39, mean 0.32), and low Fe_{Py}/Fe_{HR} (0.01–0.50, mean 0.24). These values suggest oxic conditions, an interpretation that is reinforced by low concentrations of U (up to 4 ppm, mean 2 ppm) and Mo (up to 3 ppm, mean 1 ppm) and slightly elevated V concentrations (up to 294 ppm, mean 248 ppm).

5.1.2. Redox conditions at Jinsha (outer shelf)

In Interval I, three samples have $Fe_T > 0.5\%$, variable Fe_{HR}/Fe_T (0.21–0.83, mean 0.47), and low-moderate Fe_{Py}/Fe_{HR} (0.00–0.52, mean 0.25), reflecting variably oxic to ferruginous conditions (Figs. 3A and 5B). However, the high U (up to 91 ppm, mean 37 ppm), V (up to 3792 ppm, mean 1681 ppm), and Mo concentrations (up to 90 ppm, mean 72 ppm) of Interval I samples suggest anoxic with at least intermittently euxinic conditions. The mixed redox signals can be interpreted as a consequence of fluctuating redox conditions during deposition on the Yangtze Platform (see detailed discussion in Section 5.1.5). Thus, we infer that Interval I bottomwaters were most likely deposited under dominantly ferruginous conditions with episodes of euxinia (Fig. 6B).

Interval II samples exhibit $Fe_T > 0.5\%$, variable Fe_{HR}/Fe_T (0.32–0.97, mean 0.51), and generally low Fe_{Py}/Fe_{HR} (0–0.68, mean 0.07), reflecting dominantly ferruginous conditions (Figs. 3A, 5B and 6B). However, high U (up to 54 ppm, mean 24 ppm), V (up to 2965 ppm, mean 1060 ppm), and Mo concentrations (up to 193 ppm, mean 61 ppm) suggest at least intermittent euxinia in bottomwaters. Similarly, we infer that these mixed redox signals were due to fluctuating redox conditions on the Yangtze Platform (see Section 5.1.5) and conclude that Interval II was most likely deposited under ferruginous conditions with episodes of euxinia (Fig. 6B).

Interval III samples show $Fe_T > 0.5\%$, low Fe_{HR}/Fe_T (0.08–0.48, mean 0.28), and low Fe_{Py}/Fe_{HR} (0–0.35, mean 0.01), suggesting dominantly oxic conditions (Figs. 3A and 5B). This interpretation is supported by low U (up to 7 ppm, mean 5 ppm) and Mo concentrations (up to 3 ppm, mean 1 ppm) and slightly elevated V concentrations (up to 379 ppm, mean 271 ppm).

Interval IV samples are characterized by $Fe_T > 0.5\%$, low Fe_{HR}/Fe_T (0.23–0.37, mean 0.31) and low Fe_{Py}/Fe_{HR} (0–0.37, mean 0.06), suggesting oxic bottomwaters (Figs. 5B and 6B), which is consistent with low concentrations of U (up to 6 ppm, mean 4 ppm) and Mo (up to 2 ppm, mean 1 ppm) and slightly elevated V concentrations (up to 299 ppm, mean 183 ppm) (Fig. 3A).

5.1.3. Redox conditions at Dingtai (outer shelf)

Iron speciation and RSTE data for the Dingtai section were originally reported by Xu et al. (2012). Bottomwater redox con-
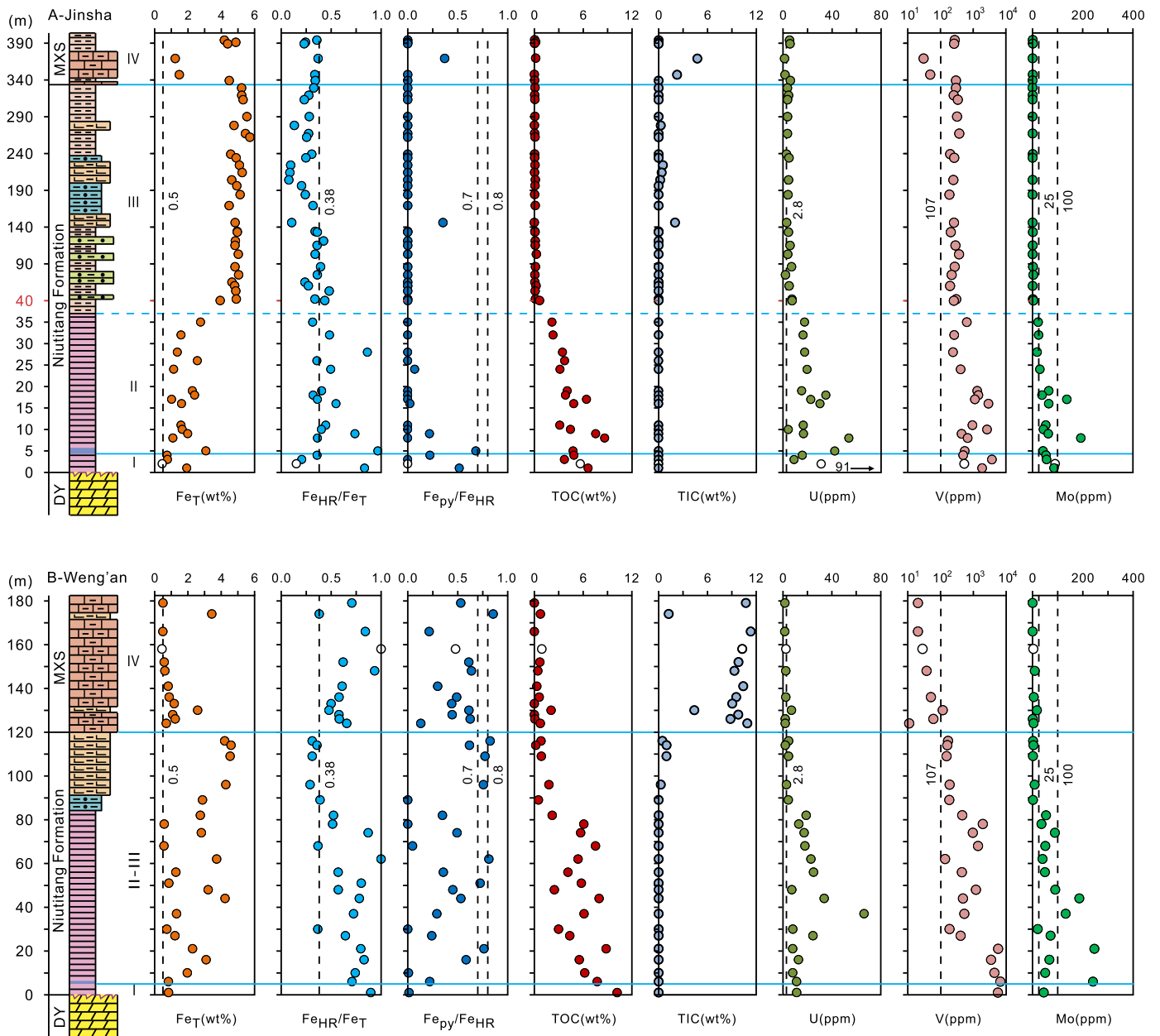
Fig. 3. Redox proxy data for (A) Jinsha and (B) Weng'an (all data original to this study). Average U (2.8 ppm) and V (107 ppm) concentrations of upper continental crust are from McLennan (2001). All samples with $Fe_T < 0.5\%$ are marked by open symbols. Vertical line(s) in each box represents key threshold value(s) discussed in text. I to IV denote stratigraphic intervals discussed in the text. Note the change in vertical scale at Jinsha (denoted by red number). Abbreviations as in Fig. 2. (For interpretation of the references to color in this figure legend, the reader is referred to the web version of this article.)

ditions were not determined for Interval I due to a lack of Fe speciation and RSTE data. In Interval II, all samples except for one with low Fe_T content are characterized by $Fe_T > 0.5\%$, variable Fe_{HR}/Fe_T (0.12–0.69, mean 0.33), and low Fe_{Py}/Fe_{HR} (0–0.14, mean 0.01), suggesting oxic to ferruginous conditions (Fig. 5C). However, high concentrations of U (up to 28 ppm, mean 18 ppm), V (up to 4400 ppm, mean 1470 ppm), and Mo (up to 394 ppm, mean 86 ppm) suggest at least intermittent euxinia. We infer that the mixed redox signals for Interval II reflect conditions that were dominantly ferruginous with episodes of euxinia (Fig. 6B; also see Section 5.1.5).

5.1.4. Redox conditions at Weng'an (outer shelf)

The only Interval I sample yields $Fe_T > 0.5\%$, high Fe_{HR}/Fe_T (0.90), low Fe_{Py}/Fe_{HR} (0.01), and relatively high concentrations of U (11 ppm), V (5610 ppm), and Mo (45 ppm), suggesting ferruginous

to euxinic conditions (Fig. 3B). Intervals II and III can be subdivided into two distinct units based on Fe speciation data (Figs. 3B and 5E). In the lower unit (6–85 m), all samples yield $Fe_T > 0.5\%$, high Fe_{HR}/Fe_T ratios (0.37–1.00, mean 0.68), and variable Fe_{Py}/Fe_{HR} ratios (0–0.81, mean 0.37), suggesting dominantly ferruginous conditions with only episodic euxinia (Fig. 6B). However, the relatively high concentrations of U (up to 67 ppm, mean 20 ppm), V (up to 6687 ppm, mean 1905 ppm), and Mo (up to 246 ppm, mean 95 ppm) are an indication of substantial bottomwater euxinia. These mixed redox signals may be the result of strongly fluctuating depositional conditions (see Section 5.1.5). In the upper unit (85–116 m), samples are characterized by $Fe_T > 0.5\%$, low Fe_{HR}/Fe_T (0.31–0.39, mean 0.33), and high Fe_{Py}/Fe_{HR} (0–0.82, mean 0.59), suggesting an oxic water column with sulfidic sediment porewaters (Fig. 6B). This interpretation is consistent with low U (up to 5 ppm, mean 4 ppm), V (up to 190 ppm, mean 172 ppm), and
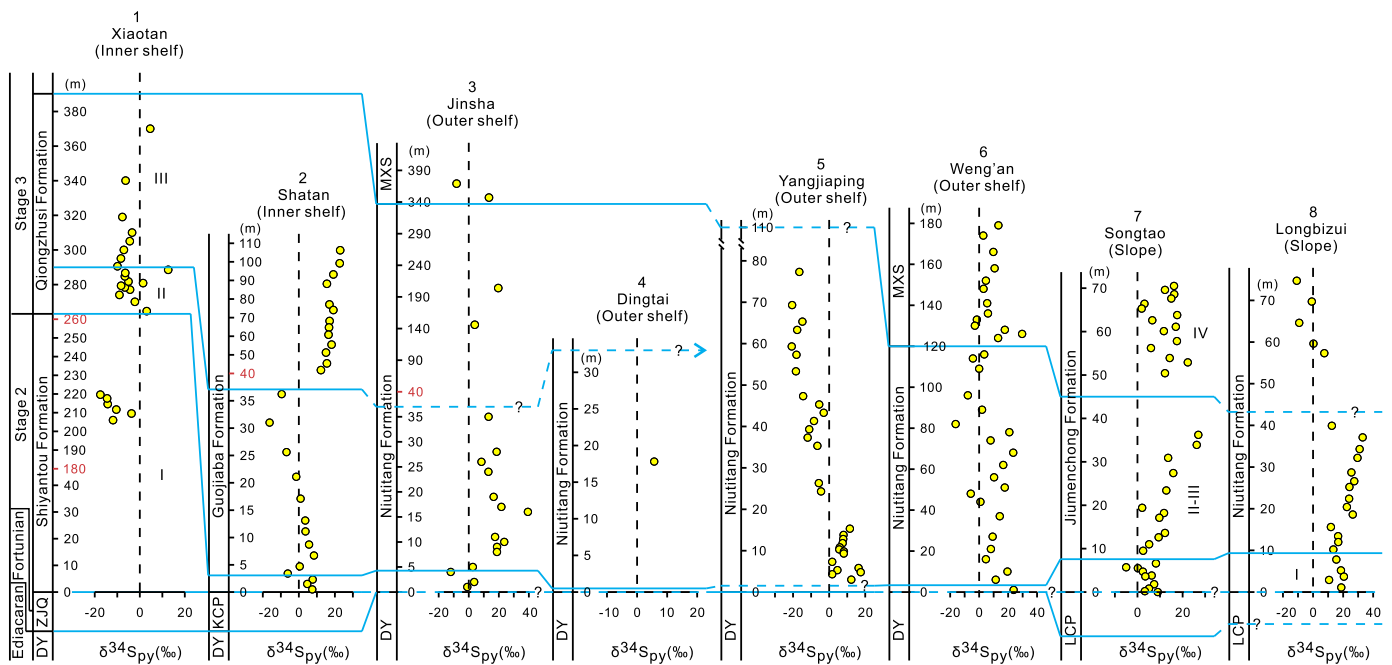
Fig. 4. Pyrite S-isotopic compositions ($\delta^{34}S_{py}$) in the eight study sections. Data sources: 1 – Xiaotan (Och et al., in press); 2 – Shatan (Goldberg et al., 2007); 3 – Jinsha (this study); 4 – Dingtai (Xu et al., 2012); 5 – Yangjiaping (Feng et al., 2014); 6 – Weng'an (this study); 7 – Songtao (Goldberg et al., 2007); 8 – Longbizui (Wang et al., 2012a). I to IV denote stratigraphic intervals discussed in the text. Note changes in the vertical scales of the Xiaotan, Shatan, and Jinsha sections (denoted by red numbers). Abbreviations as in Fig. 2. (For interpretation of the references to color in this figure legend, the reader is referred to the web version of this article.)

Mo concentrations (up to 9 ppm, mean 4 ppm). All samples in Interval IV yield $Fe_T > 0.5\%$, high Fe_{HR}/Fe_T (0.38–1.00, mean 0.65), and variable Fe_{Py}/Fe_{HR} (0.13–0.85, mean 0.49), indicating dominantly ferruginous conditions but with development of euxinia at 174 m (Fig. 6B). Although this interpretation would not seem to be supported by low U (up to 7 ppm, mean 3 ppm), V (up to 117 ppm, mean 43 ppm), and Mo concentrations (up to 18 ppm, mean 5 ppm), the low concentrations of RSTEs in Interval IV are likely due to carbonate dilution effects (total inorganic carbon up to 11.3%, mean 8.9%).

5.1.5. Recognizing intervals of fluctuating redox conditions

Many of the study sections contain stratigraphic intervals characterized by variable Fe_{HR}/Fe_T and low Fe_{Py}/Fe_{HR} ratios, suggesting dominantly oxic to anoxic–ferruginous conditions, and relatively high RSTE concentrations, suggesting anoxic–euxinic conditions (see Sections 5.1.2, 5.1.3, and 5.1.4). The reason for these apparently discordant redox signals is uncertain. As suggested by Li et al. (2012), the Fe speciation ratios may have been altered by weathering of pyrite in the original samples, possibly reflected in larger-than-usual amounts of Fe_{ox} in their Fe_{HR} pools (e.g., as for some samples from Jinsha, Yangjiaping and Weng'an; Table S1) although petrographic examination provided scant evidence of weathering. Fe speciation results may also be fundamentally less reliable in an Fe-limited system in which the Fe_T content ($\sim$ <0.5 wt.%; e.g., some samples from Jinsha and Weng'an; Table S1) begins to approach the analytical error ($\sim\pm0.1$ wt.%). Here, we propose an alternative hypothesis, that these patterns record intervals of strong redox variation, with different redox proxies under the dominant influence of different redox conditions (cf. Kenig et al., 2004). For intervals characterized by dominantly ferruginous conditions with frequent episodes of euxinia, the former (ferruginous) conditions are reflected in low Fe_{Py}/Fe_{HR} ratios, whereas the latter (euxinic) episodes are more sensitively reflected in elevated RSTE concentrations. RSTEs can be removed from the water column to the sediment rapidly when conditions permit, as in the modern Black Sea in which the aqueous concentrations of some trace metals

have been substantially depleted in <8 kyr (Morford and Emerson, 1999; Algeo and Maynard, 2008).

The pattern of Fe_{Py}/Fe_{HR} vs. Mo_{EF} covariation at Yangjiaping offers support for the interpretation of fluctuating redox conditions. Intervals II and III, which exhibit a wide range of Fe_{Py}/Fe_{HR} ratios, show a systematic shift in Mo_{EF} as a function of Fe_{Py}/Fe_{HR}: for Fe_{Py}/Fe_{HR} of <0.1, 0.1–0.9, and >0.9, Mo_{EF} yields median values of 21 (9–33, i.e., the 16th–84th percentile range), 81 (17–148), and 185 (111–286), respectively. This pattern is consistent with a shift from dominantly ferruginous conditions with infrequent euxinic episodes to ferruginous conditions with more frequent euxinic episodes, and then to dominantly euxinic conditions. If correct, then Fe_{Py}/Fe_{HR} vs. Mo_{EF} crossplots have utility for evaluating not only average redox conditions but also redox variability within paleomarine systems. The lack of strong positive covariation between Fe_{Py}/Fe_{HR} and Mo_{EF} for most of the present study sections (Fig. 7) suggests that high-frequency redox variations may have been the norm on the early Cambrian Yangtze Block.

5.1.6. Synthesis: spatiotemporal variability in redox conditions on the early Cambrian Yangtze Block

Detailed examination of Fe speciation and redox-sensitive trace element data in the four sections discussed above, together with the same types of data from the Shatan (inner shelf), Yangjiaping (outer shelf), Songtao (slope), Longbizui (slope) sections as discussed by Feng et al. (2014), provides compelling evidence for strong temporal and spatial variability of ocean redox conditions on the early Cambrian Yangtze Block (Figs. 5 and 6). This interpretation is consistent with the conclusions of earlier studies that the highly heterogeneous redox conditions of the late Neoproterozoic oceans persisted into the early Cambrian (e.g., Feng et al., 2014). One important point to note is that redox patterns on the early Cambrian Yangtze Block are related to sediment lithology only to a limited degree. Although there is a modest tendency for carbonates to be associated with oxic conditions and for shales to be associated with ferruginous or euxinic conditions, each lithology
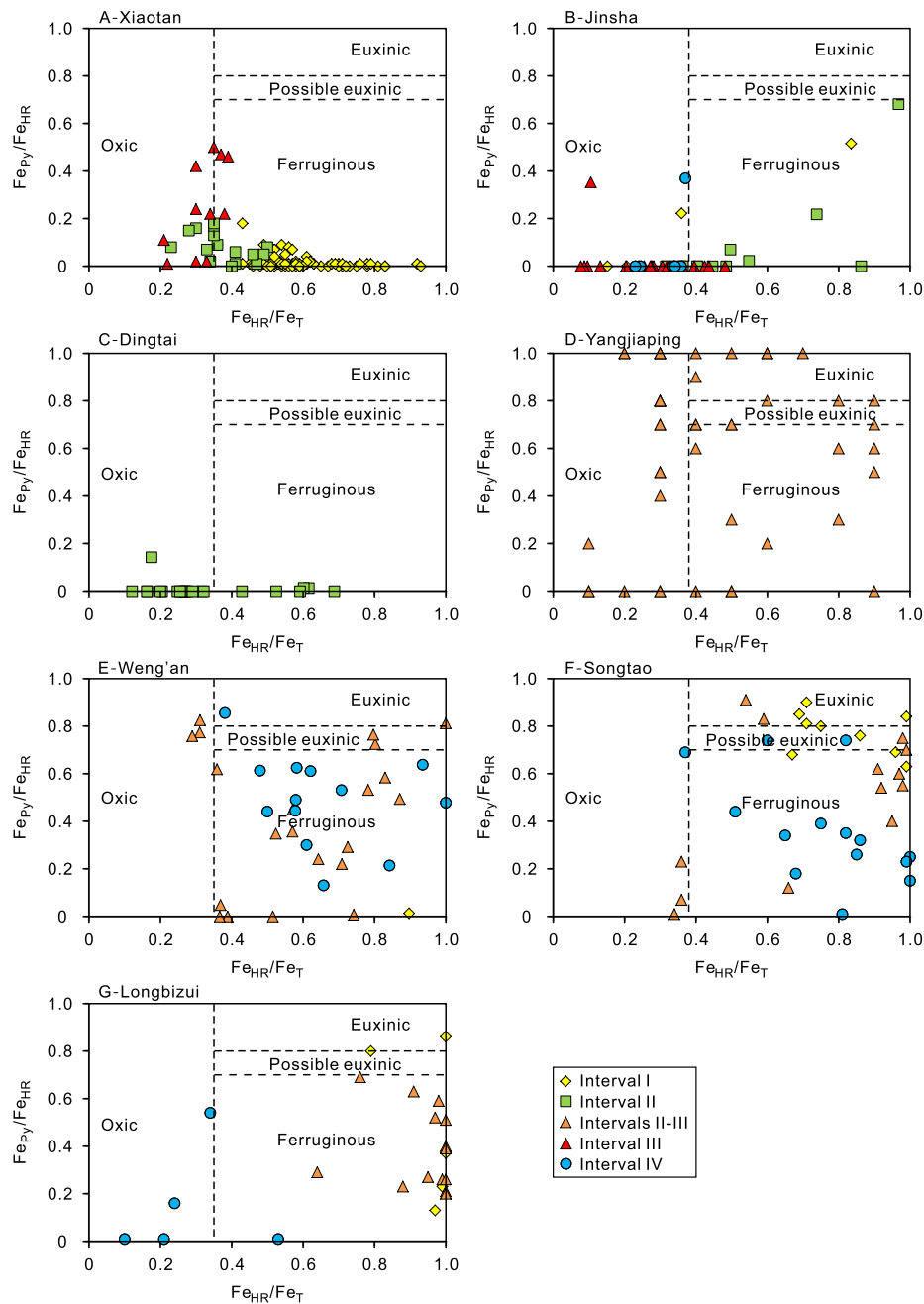
Fig. 5. Fe_{HR}/Fe_T vs. Fe_{Py}/Fe_{HR} for seven of the study sections (no Fe-speciation data available for Shatan). The divisions between oxic and anoxic conditions ($Fe_{HR}/Fe_T = 0.38$) and between ferruginous–anoxic and euxinic–anoxic conditions ($Fe_{Py}/Fe_{HR} = 0.7–0.8$) are based on Poulton and Canfield (2011). Data sources as in Fig. 4 except for Songtao (Canfield et al., 2008).

accumulated under a range of redox conditions, and lithology does not appear to be a dominant control over redox patterns (Fig. 8).

Our synthesis of redox patterns in eight sections representing a spectrum of shallow to deep facies along two intersecting transects across the Yangtze Block (Fig. 1B) demonstrates that euxinic waters dynamically coexisted at intermediate depths with oxygenated surface waters and ferruginous deep waters (Figs. 5 and 6). This spatial pattern of redox variation, which has been previously reported for the Precambrian (Li et al., 2010; Poulton et al., 2010; Planavsky et al., 2011; Poulton and Canfield, 2011), has been termed the "euxinic wedge model" (Li et al., 2010, 2015). The spatiotemporal extent of development of oceanic euxinic wedges is uncertain at present, and there are clearly boundary conditions specific to the early Cambrian Yangtze Block that contributed to

its development there, i.e., (1) improved ventilation of the ocean-surface layer owing to increasing atmospheric oxygen levels during the Ediacaran–Cambrian transition, and (2) ferruginous deep-water conditions owing to hydrothermal emanations of reduced Fe from the deep Nanhua Basin (e.g., Wang et al., 2012b).

Our reconstruction of ocean redox conditions on the early Cambrian Yangtze Block suggests three steps of increased oxygenation (Fig. 6). The first step occurred at the Interval I/II boundary and was marked by a transition from transient oxic episodes to persistently oxic conditions at the inner-shelf Xiaotan section but a continuation of mostly anoxic conditions at the other seven study sections. The second step coincided with the Interval II/III boundary and resulted in an extension of persistently oxic conditions from the inner-shelf Xiaotan to the outer-shelf Jinsha section and,
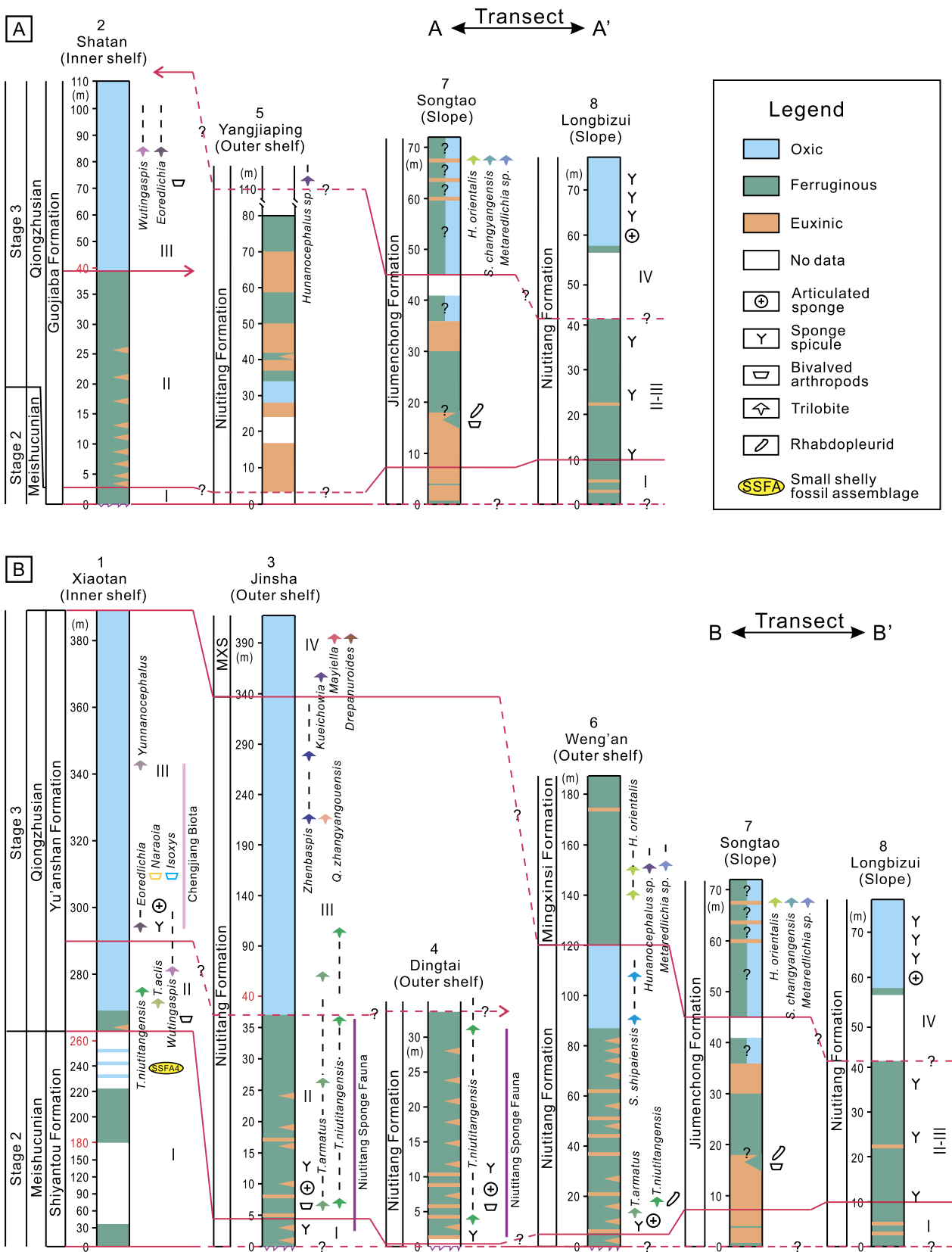
Fig. 6. Spatiotemporal variations in watermass redox conditions along two shelf-to-basin transects (see Fig. 1B), as determined by Fe-speciation and RSTE data. See Fig. 2 for sources of biostratigraphic data and abbreviations.

possibly, the outer-shelf Weng'an section (although the position of the II/III boundary at Weng'an is uncertain). However, the slope Songtao and Longbizui sections remained largely anoxic at that time.

The third step occurred around the Interval III/IV boundary and is marked by a profound change from anoxic to oxic conditions in slope sections, i.e., with increased oxygen levels possibly
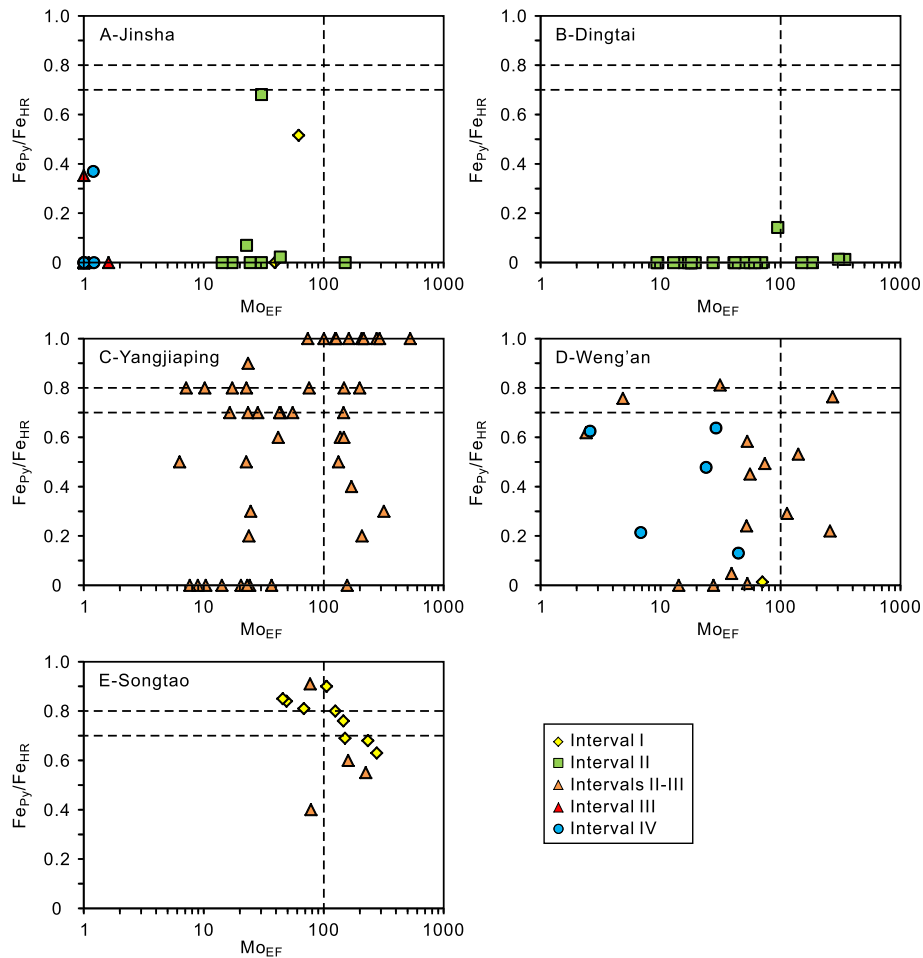
Fig. 7. Fe_{Py}/Fe_{HR} vs. Mo_{EF} for five of the study sections. The ferruginous-vs-euxinic threshold ($Fe_{Py}/Fe_{HR} = 0.7$–0.8) is from Poulton and Canfield (2011), and the 100 ppm Mo threshold separating persistently euxinic from more weakly reducing environments is from Scott and Lyons (2012). Data sources as in Figs. 4 and 5. Xiaotan, Shatan and Longbizui are not shown due to lack of data for one or more of the proxies Al, Ti, Fe_{Py}/Fe_{HR}, and Mo.

appearing somewhat earlier at Songtao (just below III/IV boundary) relative to Longbizui (above the Interval III/IV boundary; Fig. 6). These findings appear to record a stepwise expansion of oxic facies from shallower to deeper settings that began in the Qiongzhusian (i.e., Cambrian Stage 3), consistent with the oxygenation pattern of early oceans described by Li et al. (2015).

5.1.7. The highly heterogeneous redox state of the early Cambrian global ocean

Our finding of substantial heterogeneity in oceanic redox conditions during Cambrian Stages 2 and 3 in South China is consistent with the results from age-equivalent sections globally. For example, Cambrian Stages 2 and 3 (~529–514 Ma) are characterized by anoxic but non-euxinic conditions in Iran (Rajabi et al., 2015). The Cambrian Fortunian Stage (~541–529 Ma) is characterized by anoxic conditions with episodes of euxinia in Oman (Schröder and Grotzinger, 2007; Wille et al., 2008), anoxic conditions in Iran (Kimura and Watanabe, 2001), and ferruginous conditions in Canada (Sperling et al., 2015). These examples provide evidence for early Cambrian redox heterogeneity globally. This finding is consistent with low atmospheric oxygen levels (10–40% PAL) in the early Cambrian (Sperling et al., 2015), but conflicts with inferences of near-modern atmospheric oxygen levels (Berner, 2009) and complete oxygenation of the global ocean (X. Chen et al., 2015). Our observation of a stepwise increase in oceanic oxygen levels beginning in Cambrian Stage 3 is also at odds with an inferred decrease

in global oxygen levels at that time as a consequence of rising bioturbation intensity during Cambrian Stage 2 (Boyle et al., 2014).

5.2. Sulfur isotopic records

The heterogeneity of ocean chemistry during the early Cambrian is also likely to have extended to the marine sulfate reservoir. To constrain seawater sulfate concentrations during the early Cambrian, we measured the isotopic composition of pyrite ($\delta^{34}S_{Py}$) in the outer-shelf Jinsha and Weng'an sections, supplementing existing data from the inner-shelf Xiaotan (Och et al., in press), inner-shelf Shatan (Goldberg et al., 2007), outer-shelf Dingtai (Xu et al., 2012), outer-shelf Yangjiaping (Feng et al., 2014), slope Songtao (Goldberg et al., 2007), and slope Longbizui sections (Wang et al., 2012a). Our results confirm the existence of the large spatial gradient in $\delta^{34}S_{Py}$ proposed by Feng et al. (2014): for Intervals I, II–III, and IV, the $\delta^{34}S_{Py}$ of inner–outer shelf facies averages −12.0‰, −5.3‰, and +2.7‰, respectively, and that of slope facies averages +16.8‰, +22.5‰, and +12.4‰, respectively (Table 1, Fig. 4).

The spatial gradient of $\delta^{34}S_{Py}$ across the early Cambrian Yangtze Block was attributed by Feng et al. (2014) to variation in the S-isotopic composition of sulfate used in microbial sulfate reduction (MSR): (1) isotopically light riverine sulfate yielding low $\delta^{34}S_{Py}$ values in nearshore areas, and (2) isotopically heavy seawater sulfate yielding high $\delta^{34}S_{Py}$ values in offshore areas. We note that mixing of two sources of sulfate can also explain the highly variable $\delta^{34}S_{Py}$ values of Intervals II and III of the Weng'an section in this
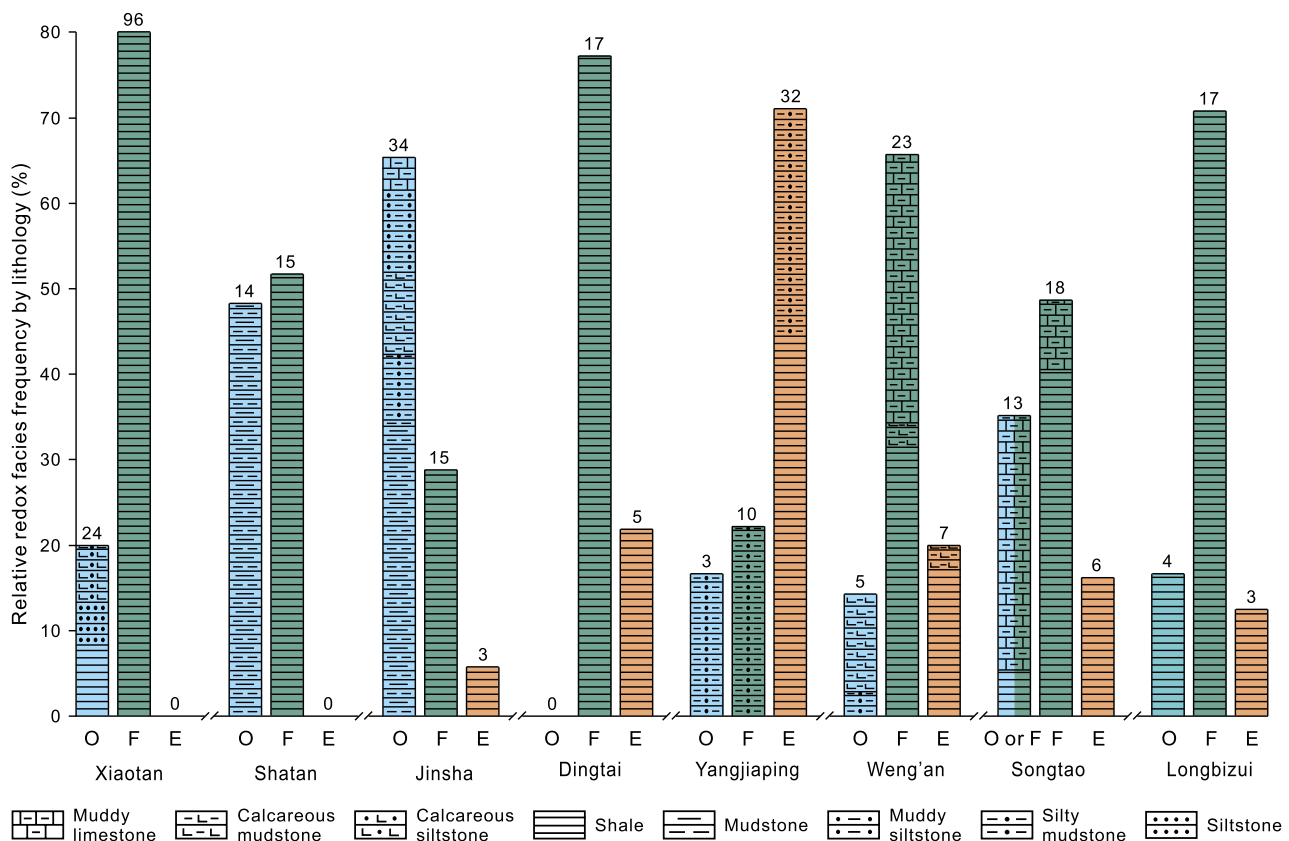
Fig. 8. Histograms showing relationship of redox conditions to lithology for the eight study sections. Abbreviations: O = Oxic, F = Ferruginous, E = Euxinic. The number above each column indicates the number of samples for each redox condition. See Section 5.1 and Feng et al. (2014) for detailed explanations of redox conditions.

Table 1
Mean pyrite sulfur isotopic compositions ($\delta^{34}S_{py}$) by stratigraphic interval and study section.

Interval	I	II	III	IV
Xiaotan (inner shelf)	−12.0 (−17.5/−3.7; $n=6$)	−2.8 (−9.0/+12.6; $n=11$)	−5.3 (−9.9/+4.7; $n=8$)	–
Shatan (inner shelf)	+6.6 (+4.7/+7.7; $n=3$)	−1.6 (−16.2/+8.4; $n=11$)	+17.6 (+12.3/+23.0; $n=13$)	–
Jinsha (outer shelf)	−3.1 (−12.0/+3.6; $n=3$)	+17.7 (+2.7/+39.4; $n=12$)	+11.8 (+4.0/+19.7; $n=2$)	+2.7 (−8.1/+13.5; $n=2$)
Dingtai (outer shelf)	–	+5.7 ($n=1$)	–	–
Yangjiaping (outer shelf)	–		−2.7 (−20.7/+17.5; $n=30$)	–
Weng'an (outer shelf)	+23.8 ($n=1$)	+7.3 (−16.2/+23.6; $n=20$)	+8.6 (−2.9/+29.7; $n=13$)
Songtao (slope)	+4.0 (−5.0/+9.0; $n=10$)	+12.4 (+2.1/+27.0; $n=12$)	+12.4 (+3.1/+22.3; $n=13$)
Longbizui (slope)	+16.8 (+10.7/+20.5; $n=5$)	+22.5 (+12.5/+33.0; $n=14$)	+1.1 (−10.8/+7.5; $n=5$)

Note: Values within parentheses are minimum/maximum values and number of samples (n).
"–" indicates no data.

study. This hypothesis implies low seawater sulfate concentrations, especially in the deep global ocean assuming a good connection of the Nanhua Basin with the open ocean (see Section 2.1).

Our results are consistent with the inference of low seawater sulfate concentrations during the early Cambrian based on sulfur isotope data from Mexico and California (<2 mM; Loyd et al., 2012) and South China (Feng et al., 2014), and halite fluid inclusions from Siberia (Petrychenko et al., 2005) and Australia (Kovalevych et al., 2006). However, the early Cambrian was a time of widespread deposition of sulfate-bearing evaporites, e.g., in Oman (Fike and Grotzinger, 2010), Russia (Claypool et al., 1980), and India (Strauss et al., 2001), and moderately high (5–10 mM) to high (>10 mM) contemporaneous seawater sulfate concentrations were inferred on the basis of sulfur isotope data by Tarhan et al. (2015) and Canfield and Farquhar (2009), respectively. A modeling study based on multiple formations with a global distribution by Algeo et al. (2015) concluded that seawater sulfate was quite variable during the late Neoproterozoic to early Cambrian, possibly owing to generally low sulfate concentrations in the global ocean

but with locally elevated levels owing to site-specific factors. This scenario is consistent with our inference of strong redox heterogeneity of the early Cambrian ocean.

5.3. Implications for biota-environment co-evolution during the early Cambrian

5.3.1. Linking oceanic redox structure and metazoan evolution

Our analysis of ocean redox conditions suggests that changes in seawater chemistry may have been linked to bio-evolutionary developments during the early Cambrian (Fig. 6). Interval I records oxic episodes at Xiaotan, where small shelly faunas appeared (Li and Xiao, 2004), but anoxic waters in the other seven sections. Interval II exhibits a thorough transition to oxic conditions at Xiaotan, accompanied by the first appearance of trilobites in nearby sections (Jinning and Maotianshan, Luo et al., 1994; Yang et al., 2003), but persistence of mainly anoxic waters in the other seven sections. However, it is worth noting that the ferruginous deeper waters were accompanied by the appearance of

the Niutitang Sponge Fauna in the Jinsha and Zhongnan sections near Dingtai (Zhu, 2010), a few trilobites at Weng'an (Yang et al., 2003), and a few sponges at Longbizui (Guo et al., 2013). During Interval III, persistently oxic waters expanded from the inner-shelf Xiaotan and Shatan to the outer-shelf Weng'an section, concurrent with the appearance of the Chengjiang Biota at multiple sections near Xiaotan (e.g., Jinning, Maotianshan) (e.g., Luo et al., 1994; Yang et al., 2003) and with the appearance of the Zunyi Biota at Zhongnan near Dingtai (Zhao et al., 1999). However, anoxic conditions persisted in the slope Songtao and Longbizui sections at that time. Interval IV is characterized by a transition from anoxic to persistently oxic conditions in the slope Longbizui section, coincident with the first appearance of trilobites at Songtao (Yang et al., 2003) and a transition from abundant sponge spicules to abundant and large-body sponges at Longbizui (Wang et al., 2012a). These parallel changes in oceanic redox conditions and metazoan evolution suggest that a stepwise increase in seawater oxygen levels on the early Cambrian Yangtze Block is consistent with a previous hypothesis that higher oxygen levels are needed to sustain more complex ecosystems, in which animals are characterized by larger bodies and more metabolically active lifestyles (Sperling et al., 2013).

5.3.2. Assessing impacts of early animals on ocean chemistry

Numerous hypotheses have been proposed concerning the influence of early animal life on ocean chemistry (e.g., Logan et al., 1995; Canfield and Farquhar, 2009; Butterfield, 2009), among which we examine two on which our results have a potential bearing. First, the appearance of mesozooplankton is proposed to have resulted in packaging of algal organic matter into more quickly sinking fecal pellets (Logan et al., 1995) and/or to have generated a grazing pressure that compelled evolution of larger export-prone eukaryotic phytoplankton (Butterfield, 2009), thus significantly enhancing the biological pump and organic matter burial and, ultimately, deep-water oxygenation (Logan et al., 1995; Butterfield, 2009). The earliest firm paleontological evidence for the appearance of macrozooplankton (i.e., bivalved arthropod *Isoxys*) and suspension-feeding mesozooplankton (i.e., anomalocarid *Tamisiocaris borealis*) is found in Cambrian Stage 3 (∼521–514 Ma; e.g., Luo et al., 1994; Vinther et al., 2014). However, deep waters remained anoxic in many basins and, possibly, globally at that time (see Section 5.1), supporting the proposal that zooplankton fecal pellets had limited effect on overall carbon export (Turner, 2002) and apparently contradicting the hypothesis that the evolution of macrozooplankton and suspension-feeding mesozooplankton initiated deep-ocean oxygenation (Logan et al., 1995; Butterfield, 2009). Second, intensified bioturbation is proposed to have increased seawater sulfate concentrations up to ∼10 mM or more by enhancing oxidation of sedimentary sulfides (Canfield and Farquhar, 2009). However, this hypothesis is inconsistent with evidence for a small seawater sulfate reservoir during the early Cambrian (see Section 5.2). Our results are consistent with the view that the influence of bioturbation on absolute sulfate concentrations was probably minor (Loyd et al., 2012; Tarhan et al., 2015). In summary, our results contradict existing hypotheses concerning a strong influence of metazoan evolution on the chemistry of early Cambrian oceans.

6. Conclusions

High-resolution Fe speciation, elemental concentration, and sulfur isotope data are reported for the outer-shelf Jinsha and Weng'an sections of the early Cambrian Yangtze Platform in South China. Our new data, combined with existing data from six other sections representing a range of paleowater depths (Xiaotan, Shatan, Dingtai, Yangjiaping, Songtao, and Longbizui), suggest that euxinic mid-depth waters were dynamically maintained between

oxic surface waters and ferruginous deep waters, and that oceanic oxygenation proceeded in a stepwise manner as oxic conditions slowly penetrated into outer-shelf and basinal environments beginning in Cambrian Stage 3 (∼521–514 Ma). Our reconstruction of early Cambrian redox conditions in South China in combination with those in sections from Oman, Iran and Canada, suggests a high degree of spatial heterogeneity in redox conditions for the early Cambrian global ocean, consistent with low atmospheric oxygen levels (∼10–40% PAL) but contrary to inferences of oxygen levels similar to the modern. A pronounced gradient in $\delta^{34}S_{py}$ suggests low concentrations and strong spatial variation in seawater sulfate, which supports our inference of low rather than high contemporaneous global-ocean sulfate levels.

Integration of information regarding marine redox conditions and fossil distributions suggests that a stepwise oxygenation of shelf and slope environments is consistent with gradual increases in ecosystem complexity during the early Cambrian. This finding implies that the "Cambrian Explosion" in South China might have been mainly a local consequence of improved surface–ocean oxygenation rather than a response to global-ocean ventilation. Furthermore, correlation of our reconstructed ocean chemistry with early Cambrian bio-evolutionary patterns reveals two surprising results: (1) the world's deep waters remained anoxic and ferruginous following the appearance of macrozooplankton and suspension-feeding mesozooplankton, and (2) the global seawater sulfate reservoir remained small despite a stepwise increase in bioturbation during the early Cambrian. These results are inconsistent with hypotheses regarding changes in ocean chemistry triggered by the appearance of mesozooplankton and a rise in bioturbation during the early Cambrian, although further studies are needed to fully explore the impact of early animals on ocean chemistry.

Appendix A. Supplementary material

Supplementary material related to this article can be found online at http://dx.doi.org/10.1016/j.epsl.2016.02.019.

References

Algeo, T.J., Maynard, J.B., 2008. Trace-metal covariation as a guide to watermass conditions in ancient anoxic marine environments. Geosphere 4, 872–887.

Algeo, T.J., Luo, G.M., Song, H.Y., Lyons, T.W., Canfield, D.E., 2015. Reconstruction of secular variation in seawater sulfate concentrations. Biogeosciences 12, 2131–2151.

Berner, R.A., 2009. Phanerozoic atmospheric oxygen: new results using the GEOCARBSULF model. Am. J. Sci. 309, 603–606.

Boyle, R.A., Dahl, T.W., Dale, A.W., Shields-Zhou, G.A., Zhu, M., Brasier, M.D., Canfield, D.E., Lenton, T.M., 2014. Stabilization of the coupled oxygen and phosphorus cycles by the evolution of bioturbation. Nat. Geosci. 7, 671–676.

Butterfield, N.J., 2009. Oxygen, animals and oceanic ventilation: an alternative view. Geobiology 7, 1–7.

Canfield, D.E., Raiswell, R., Westrich, J.T., Reaves, C.M., Berner, R.A., 1986. The use of chromium reduction in the analysis of reduced inorganic sulfur in sediments and shales. Chem. Geol. 54, 149–155.

Canfield, D.E., Poulton, S.W., Knoll, A.H., Narbonne, G.M., Ross, G., Goldberg, T., Strauss, H., 2008. Ferruginous conditions dominated later Neoproterozoic deep-water chemistry. Science 321, 949–952.

Canfield, D.E., Farquhar, J., 2009. Animal evolution, bioturbation, and the sulfate concentration of the oceans. Proc. Natl. Acad. Sci. USA 106, 8123–8127.

Chen, D., Zhou, X., Fu, Y., Wang, J., Yan, D., 2015. New U–Pb zircon ages of the Ediacaran–Cambrian boundary strata in South China. Terra Nova 27, 62–68.

Chen, J.Y., Hou, X.G., Li, G.X., 1990. New Lower Cambrian demosponges – *Quadrolaminiella gen. nov.* from Chengjiang, Yunnan. Acta Palaeontol. Sin. 29, 402–414 (in Chinese with English abstract).

Chen, X., Ling, H.F., Vance, D., Shields-Zhou, G.A., Zhu, M., Poulton, S.W., Och, L.M., Jiang, S.Y., Li, D., Cremonese, L., Archer, C., 2015. Rise to modern levels of ocean oxygenation coincided with the Cambrian radiation of animals. Nat. Commun. 6, 7142.

Clarkson, M.O., Poulton, S.W., Guilbaud, R., Wood, R.A., 2014. Assessing the utility of Fe/Al and Fe-speciation to record water column redox conditions in carbonate-rich sediments. Chem. Geol. 382, 111–122.

Claypool, G.E., Holser, W.T., Kaplan, I.R., Sakai, H., Zak, I., 1980. The age curves of sulfur and oxygen isotopes in marine sulfate and their mutual interpretation. Chem. Geol. 28, 199–260.

Compston, W., Zhang, Z., Cooper, J.A., Ma, G., Jenkins, R.J.F., 2008. Further SHRIMP geochronology on the early Cambrian of South China. Am. J. Sci. 308, 399–420.

Feng, L.J., Li, C., Huang, J., Chang, H.J., Chu, X.L., 2014. A sulfate control on marine mid-depth euxinia on the early Cambrian (ca. 529–521 Ma) Yangtze platform, South China. Precambrian Res. 246, 123–133.

Fike, D.A., Grotzinger, J.P., 2010. A $\delta^{34}S_{SO_4}$ approach to reconstructing biogenic pyrite burial in carbonate-evaporite basins: an example from the Ara Group, Sultanate of Oman. Geology 38, 371–374.

Goldberg, T., Strauss, H., Guo, Q., Liu, C., 2007. Reconstructing marine redox conditions for the Early Cambrian Yangtze Platform: evidence from biogenic sulphur and organic carbon isotopes. Palaeogeogr. Palaeoclimatol. Palaeoecol. 254, 175–193.

Guo, Q., Shields, G., Liu, C., Strauss, H., Zhu, M., Pi, D., Goldberg, T., Yang, X., 2007. Trace element chemostratigraphy of two Ediacaran–Cambrian successions in South China: implications for organosedimentary metal enrichment and silicification in the Early Cambrian. Palaeogeogr. Palaeoclimatol. Palaeoecol. 254, 194–216.

Guo, Q., Strauss, H., Zhu, M., Zhang, J., Yang, X., Lu, M., Zhao, F., 2013. High resolution organic carbon isotope stratigraphy from a slope to basinal setting on the Yangtze Platform, South China: implications for the Ediacaran–Cambrian transition. Precambrian Res. 225, 209–217.

Ishikawa, T., Ueno, Y., Komiya, T., Sawaki, Y., Han, J., Shu, D., Li, Y., Maruyama, S., Yoshida, N., 2008. Carbon isotope chemostratigraphy of a Precambrian/Cambrian boundary section in the Three Gorge area, South China: prominent global-scale isotope excursions just before the Cambrian Explosion. Gondwana Res. 14, 193–208.

Kendall, B., Komiya, T., Lyons, T.W., Bates, S.M., Gordon, G.W., Romaniello, S.J., Jiang, G., Creaser, R.A., Xiao, S., McFadden, K., Sawaki, Y., Tahata, M., Shu, D., Han, J., Li, Y., Chu, X., Anbar, A.D., 2015. Uranium and molybdenum isotope evidence for an episode of widespread ocean oxygenation during the late Ediacaran Period. Geochim. Cosmochim. Acta 156, 173–193.

Kenig, F., Hudson, J.D., Damsté, J.S.S., Popp, B.N., 2004. Intermittent euxinia: reconciliation of a Jurassic black shale with its biofacies. Geology 32, 421–424.

Kimura, H., Watanabe, Y., 2001. Oceanic anoxia at the Precambrian–Cambrian boundary. Geology 29, 995–998.

Knoll, A.H., Carroll, S.B., 1999. Early animal evolution: emerging views from comparative biology and geology. Science 284, 2129–2137.

Kovalevych, V., Zang, W.-L., Peryt, T., Khmelevska, O., Halas, S., Iwasinska-Budzyk, I., Boult, P., Heithersay, P., 2006. Deposition and chemical composition of Early Cambrian salt in the eastern Officer Basin, South Australia. Aust. J. Earth Sci. 53, 577–593.

Landing, E., Geyer, G., Brasier, M.D., Bowring, S.A., 2013. Cambrian Evolutionary Radiation: context, correlation, and chronostratigraphy—overcoming deficiencies of the first appearance datum (FAD) concept. Earth-Sci. Rev. 123, 133–172.

Lenniger, M., Nøhr-Hansen, H., Hills, L.V., Bjerrum, C.J., 2014. Arctic black shale formation during Cretaceous Oceanic Anoxic Event 2. Geology 42, 799–802.

Li, C., Love, G.D., Lyons, T.W., Fike, D.A., Sessions, A.L., Chu, X., 2010. A stratified redox model for the Ediacaran ocean. Science 328, 80–83.

Li, C., Love, G.D., Lyons, T.W., Scott, C.T., Feng, L., Huang, J., Chang, H., Zhang, Q., Chu, X., 2012. Evidence for a redox stratified Cryogenian marine basin, Datangpo Formation, South China. Earth Planet. Sci. Lett. 331–332, 246–256.

Li, C., Cheng, M., Algeo, T.J., Xie, S.C., 2015. A theoretical prediction of chemical zonation in early oceans (>520 Ma). Sci. China Earth Sci. 58, 1901–1909.

Li, G., Xiao, S., 2004. Tannuolina and Micrina (Tannuolinidae) from the Lower Cambrian of eastern Yunnan, South China, and their scleritome reconstruction. J. Paleontol. 78, 900–913.

Li, Z.-X., Bogdanova, S., Collins, A., Davidson, A., De Waele, B., Ernst, R., Fitzsimons, I., Fuck, R., Gladkochub, D., Jacobs, J., 2008. Assembly, configuration, and break-up history of Rodinia: a synthesis. Precambrian Res. 160, 179–210.

Logan, G.A., Hayes, J., Hieshima, G.B., Summons, R.E., 1995. Terminal Proterozoic reorganization of biogeochemical cycles. Nature 376, 53–56.

Loyd, S.J., Marenco, P.J., Hagadorn, J.W., Lyons, T.W., Kaufman, A.J., Sour-Tovar, F., Corsetti, F.A., 2012. Sustained low marine sulfate concentrations from the Neoproterozoic to the Cambrian: insights from carbonates of northwestern Mexico and eastern California. Earth Planet. Sci. Lett. 339–340, 79–94.

Luo, H.L., Jiang, Z.W., Tang, L.D., 1994. Stratotype Section for Lower Cambrian Stages in China. Yunnan Science and Technology Press, Kunming, China (in Chinese with English abstract).

Luo, H.L., Hu, S.X., Zhang, S.H., Tao, Y.H., 1997. New occurrence of the Early Cambrian Chengjiang fauna in Haikou, Kunming, Yunnan province, and study on trilobitoidea. Acta Geol. Sin. 71, 122–132 (English version).

Lyons, T.W., Severmann, S., 2006. A critical look at iron paleoredox proxies: new insights from modern euxinic marine basins. Geochim. Cosmochim. Acta 70, 5698–5722.

McLennan, S.M., 2001. Relationships between the trace element composition of sedimentary rocks and upper continental crust. Geochem. Geophys. Geosyst. 2, 2000GC000109.

Mills, D.B., Canfield, D.E., 2014. Oxygen and animal evolution: did a rise of atmospheric oxygen "trigger" the origin of animals? BioEssays 36, 1145–1155.

Morford, J.L., Emerson, S., 1999. The geochemistry of redox sensitive trace metals in sediments. Geochim. Cosmochim. Acta 63, 1735–1750.

Och, L.M., Shields-Zhou, G.A., Poulton, S.W., Manning, C., Thirlwall, M.F., Li, D., Chen, X., Ling, H., Osborn, T., Cremonese, L., 2013. Redox changes in Early Cambrian black shales at Xiaotan section, Yunnan Province, South China. Precambrian Res. 225, 166–189.

Och, L.M., Cremonese, L., Shields-Zhou, G.A., Poulton, S.W., Struck, U., Ling, H., Li, D., Chen, X., Manning, C., Thirlwall, M., Strauss, H., Zhu, M., in press. Palaeoceanographic controls on spatial redox distribution over the Yangtze Platform during the Ediacaran–Cambrian transition. Sedimentology. http://dx.doi.org/10.1111/sed.12220.

Petrychenko, O.Y., Peryt, T.M., Chechel, E.I., 2005. Early Cambrian seawater chemistry from fluid inclusions in halite from Siberian evaporites. Chem. Geol. 219, 149–161.

Planavsky, N.J., McGoldrick, P., Scott, C.T., Li, C., Reinhard, C.T., Kelly, A.E., Chu, X., Bekker, A., Love, G.D., Lyons, T.W., 2011. Widespread iron-rich conditions in the mid-Proterozoic ocean. Nature 477, 448–451.

Poulton, S.W., Canfield, D.E., 2005. Development of a sequential extraction procedure for iron: implications for iron partitioning in continentally derived particulates. Chem. Geol. 214, 209–221.

Poulton, S.W., Fralick, P.W., Canfield, D.E., 2010. Spatial variability in oceanic redox structure 1.8 billion years ago. Nat. Geosci. 3, 486–490.

Poulton, S.W., Canfield, D.E., 2011. Ferruginous conditions: a dominant feature of the ocean through Earth's history. Elements 7, 107–112.

Raiswell, R., Canfield, D.E., 1998. Sources of iron for pyrite formation in marine sediments. Am. J. Sci. 298, 219–245.

Rajabi, A., Canet, C., Rastad, E., Alfonso, P., 2015. Basin evolution and stratigraphic correlation of sedimentary-exhalative Zn–Pb deposits of the Early Cambrian Zarigan–Chahmir Basin, Central Iran. Ore Geol. Rev. 64, 328–353.

Schröder, S., Grotzinger, J., 2007. Evidence for anoxia at the Ediacaran–Cambrian boundary: the record of redox-sensitive trace elements and rare earth elements in Oman. J. Geol. Soc. (Lond.) 164, 175–187.

Scott, C., Lyons, T.W., 2012. Contrasting molybdenum cycling and isotopic properties in euxinic versus non-euxinic sediments and sedimentary rocks: refining the paleoproxies. Chem. Geol. 324–325, 19–27.

Shu, D., Isozaki, Y., Zhang, X., Han, J., Maruyama, S., 2014. Birth and early evolution of metazoans. Gondwana Res. 25, 884–895.

Sperling, E.A., Frieder, C.A., Raman, A.V., Girguis, P.R., Levin, L.A., Knoll, A.H., 2013. Oxygen, ecology, and the Cambrian radiation of animals. Proc. Natl. Acad. Sci. USA 110, 13446–13451.

Sperling, E.A., Wolock, C.J., Morgan, A.S., Gill, B.C., Kunzmann, M., Halverson, G.P., Macdonald, F.A., Knoll, A.H., Johnston, D.T., 2015. Statistical analysis of iron geochemical data suggests limited late Proterozoic oxygenation. Nature 523, 451–454.

Steiner, M., Li, G., Qian, Y., Zhu, M., Erdtmann, B.D., 2007. Neoproterozoic to early Cambrian small shelly fossil assemblages and a revised biostratigraphic correlation of the Yangtze Platform (China). Palaeogeogr. Palaeoclimatol. Palaeoecol. 254, 67–99.

Strauss, H., Banerjee, D.M., Kumar, V., 2001. The sulfur isotopic composition of Neoproterozoic to early Cambrian seawater—evidence from the cyclic Hanseran evaporites, NW India. Chem. Geol. 175, 17–28.

Tarhan, L.G., Droser, M.L., Planavsky, N.J., Johnston, D.T., 2015. Protracted development of bioturbation through the early Palaeozoic Era. Nat. Geosci. 8, 865–869.

Thomson, D., Rainbird, R.H., Planavsky, N., Lyons, T.W., Bekker, A., 2015. Chemostratigraphy of the Shaler Supergroup, Victoria Island, NW Canada: a record of ocean composition prior to the Cryogenian glaciations. Precambrian

Res. 263, 232–245.

Tribovillard, N., Algeo, T.J., Lyons, T., Riboulleau, A., 2006. Trace metals as paleoredox and paleoproductivity proxies: an update. Chem. Geol. 232, 12–32.

Turner, E., Bekker, A., 2016. Thick sulfate evaporite accumulations marking a mid-Neoproterozoic oxygenation event (Ten Stone Formation, Northwest Territories, Canada). Geol. Soc. Am. Bull. 128, 203–222.

Turner, J.T., 2002. Zooplankton fecal pellets, marine snow and sinking phytoplankton blooms. Aquat. Microb. Ecol. 27, 57–102.

Vannier, J., Liu, J., Lerosey-Aubril, R., Vinther, J., Daley, A.C., 2014. Sophisticated digestive systems in early arthropods. Nat. Commun. 5, 3641.

Vinther, J., Stein, M., Longrich, N.R., Harper, D.A.T., 2014. A suspension-feeding anomalocarid from the Early Cambrian. Nature 507, 496–499.

Wang, H., Li, C., Hu, C., Xie, S., 2015. Spurious thermoluminescence characteristics of the Ediacaran Doushantuo Formation (ca. 635–551 Ma) and its implications for marine dissolved organic carbon reservoir. J. Earth Sci. 26, 883–892.

Wang, J., Li, Z.X., 2003. History of Neoproterozoic rift basins in South China: implications for Rodinia break-up. Precambrian Res. 122, 141–158.

Wang, J., Chen, D., Yan, D., Wei, H., Xiang, L., 2012a. Evolution from an anoxic to oxic deep ocean during the Ediacaran–Cambrian transition and implications for bioradiation. Chem. Geol. 306–307, 129–138.

Wang, J., Chen, D., Wang, D.A.N., Yan, D., Zhou, X., Wang, Q., 2012b. Petrology and geochemistry of chert on the marginal zone of Yangtze Platform, western Hunan, South China, during the Ediacaran–Cambrian transition. Sedimentology 59, 809–829.

Wille, M., Nagler, T.F., Lehmann, B., Schroder, S., Kramers, J.D., 2008. Hydrogen sulphide release to surface waters at the Precambrian/Cambrian boundary. Nature 453, 767–769.

Xu, L., Lehmann, B., Mao, J., Qu, W., Andao, D., 2011. Re–Os age of polymetallic Ni–Mo–PGE–Au mineralization in early Cambrian black shales of South China—a reassessment. Econ. Geol. 106, 511–522.

Xu, L., Lehmann, B., Mao, J., Nägler, T.F., Neubert, N., Böttcher, M.E., Escher, P., 2012. Mo isotope and trace element patterns of Lower Cambrian black shales in South China: multi-proxy constraints on the paleoenvironment. Chem. Geol. 318–319, 45–59.

Yang, A., Zhu, M., Zhang, J., Li, G., 2003. Early Cambrian eodiscoid trilobites of the Yangtze Platform and their stratigraphic implications. Prog. Nat. Sci. 13, 861–866.

Yang, X.L., Zhao, Y., Wu, W., Zheng, H., Zhu, Y., 2014. *Phragmodictya jinshaensis* sp. nov., a hexactinellid dictyosponge from the Cambrian of Jinsha, South China. Gff 136, 309–313.

Yin, G.Z., He, T.G., Qian, Y., Xiao, B., 1999. Geological and geographical distribution of SSF, with discussion on Early Cambrian geographical provinces. In: Qian, Y. (Ed.), Taxonomy and Biostratigraphy of Small Shelly Fossils in China. Science Press, Beijing, pp. 234–240 (in Chinese with English abstract).

Yuan, J.L., Zhao, Y.L., 1999. Subdivision and correlation of Lower Cambrian in southwest China, with a discussion of the age of Early Cambrian series biota. Acta Palaeontol. Sin. 38 (Sup.), 116–131 (in Chinese with English abstract).

Zhang, W.T., Yuan, K.X., Zhou, Z.Y., Qian, Y., Wang, Z.Z., 1979. Cambrian of southwest China. In: Nanjing Institute of Geology and Palaeontology, Chinese Academy of Sciences (Eds.), Biostratigraphy of Carbonates of Southwest China. Science Press, pp. 39–107 (in Chinese).

Zhao, Y.L., Steiner, M., Yang, R.D., Erdtmann, B.D., Guo, Q.J., Zhou, Z., Wallis, E., 1999. Discovery and significance of the early metazoan biotas from the lower Cambrian Niutitang Formation Zunyi, Guizhou, China. Acta Palaeontol. Sin. 38 (Sup.), 132–146 (in Chinese with English abstract).

Zheng, H.L., Yang, X.Y., Zhao, Y.L., Zhu, Y.J., He, S.X., 2014. Stratigraphic significance of eodiscoide from the Niutitang Formation (Cambrian) in Jinsha county, Guizhou Province. J. Guizhou Univ. (Nat. Sci.) 31, 32–37 (in Chinese with English abstract).

Zhu, M.Y., 2010. The origin and Cambrian explosion of animals: fossil evidence from China. Acta Palaeontol. Sin. 49, 269–287 (in Chinese with English abstract).

Zhu, M.Y., Zhang, J., Steiner, M., Yang, A., Li, G., Erdtmann, B.D., 2003. Sinian–Cambrian stratigraphic framework for shallow- to deep-water environments of the Yangtze Platform: an integrated approach. Prog. Nat. Sci. 13, 951–960.